



Low-amplitude Solar-like Oscillations in the K5 V Star ϵ Indi A

Mia S. Lundkvist¹, Hans Kjeldsen^{1,2}, Timothy R. Bedding³, Mark J. McCaughrean⁴, R. Paul Butler⁵, Ditte Slumstrup^{6,7}, Tiago L. Campante^{8,9}, Conny Aerts¹⁰, Torben Arentoft¹, Hans Bruntt¹, Cátia V. Cardoso¹¹, Fabien Carrier¹⁰, Laird M. Close¹², João Gomes da Silva⁸, Thomas Kallinger¹³, Robert R. King^{14,18}, Yaguang Li (李亚光)¹⁵, Simon J. Murphy¹⁶, Jakob L. Rørsted^{1,2}, and Dennis Stello¹⁷

¹ Stellar Astrophysics Centre, Department of Physics and Astronomy, Aarhus University, 8000 Aarhus C, Denmark; lundkvist@phys.au.dk

² Aarhus Space Centre (SpaCe), Department of Physics and Astronomy, Aarhus University, Denmark

³ Sydney Institute for Astronomy, School of Physics, University of Sydney NSW 2006, Australia

⁴ European Space Agency, ESTEC, Postbus 299, 2200 AG Noordwijk, The Netherlands

⁵ Earth and Planets Laboratory, Carnegie Institution for Science, 5241 Broad Branch Road, NW, Washington, DC 20015-1305, USA

⁶ European Southern Observatory, Alonso de Cordova 3107, Vitacura, Santiago, Chile

⁷ Instituto de Estudios Astrofísicos, Facultad de Ingeniería y Ciencias, Universidad Diego Portales, Av. Ejército Libertador 441, Santiago, Chile

⁸ Instituto de Astrofísica e Ciências do Espaço, Universidade do Porto, Rua das Estrelas, 4150-762 Porto, Portugal

⁹ Departamento de Física e Astronomia, Faculdade de Ciências da Universidade do Porto, Rua do Campo Alegre, s/n, 4169-007 Porto, Portugal

¹⁰ Institute of Astronomy, Department of Physics and Astronomy, KU Leuven, Celestijnenlaan 200 D, 3001 Leuven, Belgium

¹¹ Aurora Technology B.V. for ESA, ESTEC, Keplerlaan 1, 2200 AG Noordwijk, The Netherlands

¹² Department of Astronomy, University of Arizona, 933 N. Cherry Avenue, Tucson, AZ 85718, USA

¹³ Institute of Astrophysics, University of Vienna, 1180 Vienna, Austria

¹⁴ School of Physics, University of Exeter, Stocker Road, Exeter EX4 4QL, UK

¹⁵ Institute for Astronomy, University of Hawai'i, Honolulu, HI 96822, USA

¹⁶ Centre for Astrophysics, University of Southern Queensland, Toowoomba, QLD 4350, Australia

¹⁷ School of Physics, University of New South Wales, Sydney, NSW 2052, Australia

Received 2023 December 18; revised 2024 February 1; accepted 2024 February 1; published 2024 March 21

Abstract

We have detected solar-like oscillations in the mid-K-dwarf ϵ Indi A, making it the coolest dwarf to have measured oscillations. The star is noteworthy for harboring a pair of brown dwarf companions and a Jupiter-type planet. We observed ϵ Indi A during two radial velocity campaigns, using the high-resolution spectrographs HARPS (2011) and UVES (2021). Weighting the time series, we computed the power spectra and established the detection of solar-like oscillations with a power excess located at $5265 \pm 110 \mu\text{Hz}$ —the highest frequency solar-like oscillations so far measured in any star. The measurement of the center of the power excess allows us to compute a stellar mass of $0.782 \pm 0.023 M_{\odot}$ based on scaling relations and a known radius from interferometry. We also determine the amplitude of the peak power and note that there is a slight difference between the two observing campaigns, indicating a varying activity level. Overall, this work confirms that low-amplitude solar-like oscillations can be detected in mid-K-type stars in radial velocity measurements obtained with high-precision spectrographs.

Unified Astronomy Thesaurus concepts: [Astroseismology \(73\)](#); [Radial velocity \(1332\)](#); [K dwarf stars \(876\)](#)

1. Introduction

Astroseismology, the study of stellar oscillations, has flourished in recent years thanks largely to the success of the space missions Convection, Rotation, and planetary Transits (CoRoT; Baglin et al. 2006a, 2006b; Auvergne et al. 2009), *Kepler* (Borucki et al. 2010; Gilliland et al. 2010; Koch et al. 2010; Chaplin et al. 2011a), and Transiting Exoplanet Survey Satellite (TESS; Ricker et al. 2015). These satellites delivered high-quality photometric times series that are excellent for astroseismology. However, for bright Sun-like stars, radial velocity (RV) observations with a ground-based telescope can deliver a better signal-to-noise ratio (S/N), due to the much lower stellar granulation background. This is particularly true for cool main-sequence stars, where the oscillation amplitudes are very low (Kjeldsen et al. 2008; Huber et al. 2011).

¹⁸ Now at Met Office, UK.

In the case of solar-like oscillations, the overall frequency pattern is governed by two so-called global asteroseismic parameters, namely the large frequency separation ($\Delta\nu$) and the frequency of maximum power (ν_{\max}). These two parameters describe the overall regularity in the frequency comb and the location of the stellar oscillations, respectively, and they are often used to determine fundamental parameters of main-sequence and red-giant stars (see reviews by Chaplin & Miglio 2013; Hekker & Christensen-Dalsgaard 2017; García & Ballot 2019; Jackiewicz 2021).

Here, we report the detection of solar-like oscillations in the K5 V star ϵ Indi A (HD 209100). ϵ Indi A is orbited every ~ 45 yr by a Jovian mass exoplanet, ϵ Indi Ab, which has been detected in both RV and astrometry (Feng et al. 2019). ϵ Indi Ab is the nearest cold Jupiter-type planet to Earth and its infrared emission is expected to be sufficiently high to be measured by JWST (Feng et al. 2023).

In addition, ϵ Indi A is part of a hierarchical triple system with the brown dwarfs ϵ Indi Ba and ϵ Indi Bb, which have been extensively studied (see, for example, Scholz et al. 2003; Smith et al. 2003; McCaughrean et al. 2004; Roellig et al. 2004; Mainzer et al. 2007; Reiners et al. 2007; Kasper et al. 2009;

Original content from this work may be used under the terms of the [Creative Commons Attribution 4.0 licence](#). Any further distribution of this work must maintain attribution to the author(s) and the title of the work, journal citation and DOI.

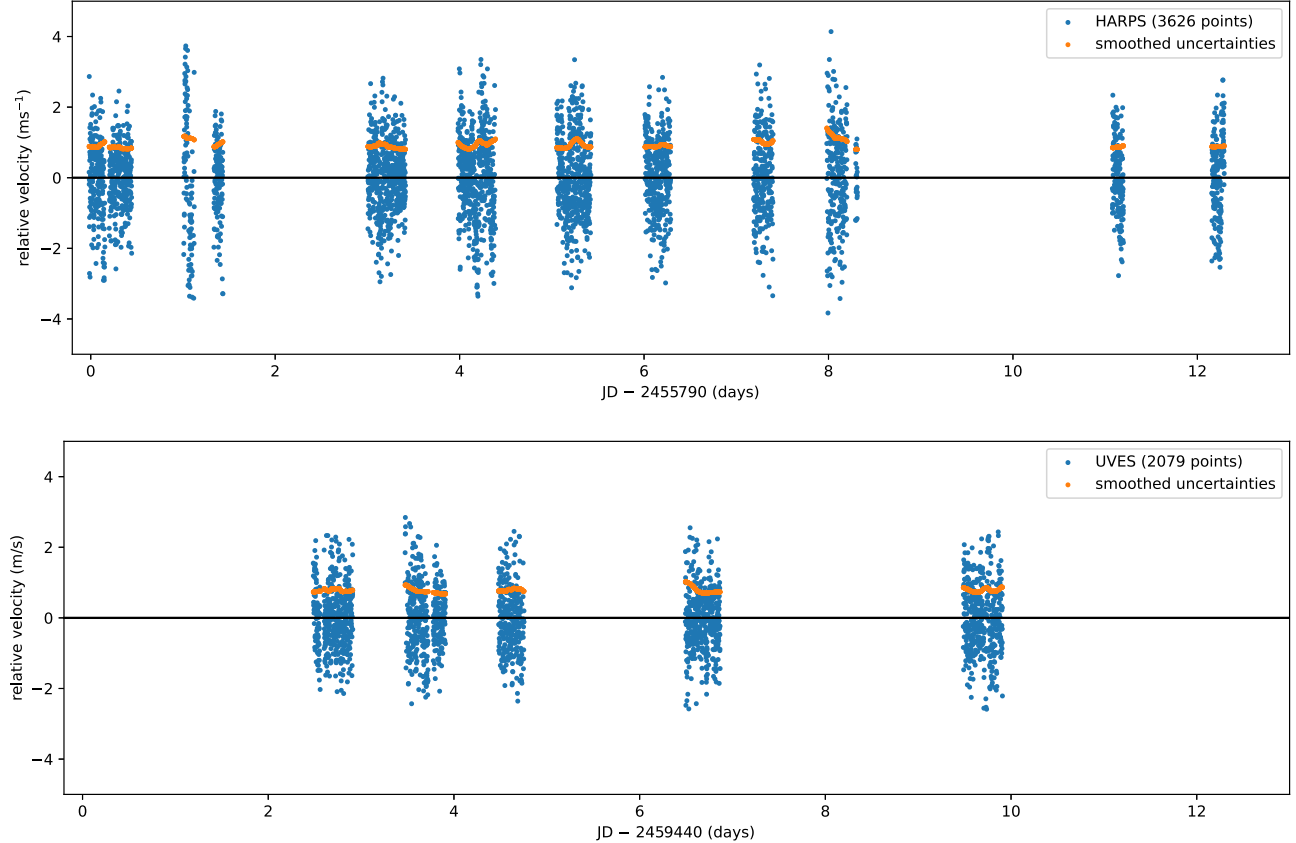


Figure 1. Radial velocity time series of ϵ Indi A from HARPS (2011 August) and UVES (2021 August). The orange points show the smoothed uncertainties that were measured from the scatter and used for weights when calculating the power spectra (see Section 3.1).

Cardoso et al. 2010; King et al. 2010; Chen et al. 2022). With the current determined dynamical masses of $66.92 \pm 0.36 M_{\text{Jup}}$ and $53.25 \pm 0.29 M_{\text{Jup}}$ for the brown dwarfs (Chen et al. 2022), as well as an accurate distance, these are among the best-characterized brown dwarfs (Chen et al. 2022). Thereby, the ϵ Indi system is highly valuable to put constraints on formation and evolution in the substellar regime (Joergens & Reffert 2014; Feng et al. 2019). However, there is disagreement over the age of the system, with estimates spanning a range 0.39–5 Gyr (Cannon 1970; Lachaume et al. 1999; Rocha-Pinto et al. 2002; Barnes 2007; Kasper et al. 2009; King et al. 2010; Dieterich et al. 2018; Feng et al. 2019; Pathak 2021; Viswanath et al. 2021; Chen et al. 2022), leaving the age to be firmly pinned down.

In Section 2 we present our RV observations and the spectroscopic analysis. The analysis of the time series with respect to asteroseismology is the topic of Section 3, while the results are presented and discussed in Section 4. The conclusion follows in Section 5.

2. Observational Data

We observed ϵ Indi A in two intensive RV campaigns separated in time by about 10 yr. The first campaign was carried out with HARPS in 2011, while a UVES campaign followed in 2021. It should be noted that ϵ Indi A fell in the TESS field in Sectors 1 and 27 and was observed photometrically in the 2 minute cadence mode for ~ 27 days each. It was also observed by TESS with 20 s cadence in Sector 68.

However, the oscillations are not visible in any of these data, which is to be expected given their small amplitudes.

2.1. HARPS RV Data

The data were collected over 12 nights in 2011 August with HARPS on the ESO 3.6 m telescope at La Silla Observatory, Chile. Around 40% of the time was lost due to bad weather. The median exposure time was 30 s, sometimes increased to 35 s or 40 s in poorer conditions. The exposure time was kept short due to the high expected frequency of the oscillations. The readout time between each exposure was 32 s, and hence the median sampling time was 62 s (which corresponds to a Nyquist frequency of about 8000 μ Hz).

For this work, we used the RVs derived by Trifonov et al. (2020) as part of the correction of public HARPS data for systematic errors. A plot of the RV time series can be found in the top panel of Figure 1.

2.2. UVES RV Data

In 2021 August we observed ϵ Indi A during six nonconsecutive (5+1) nights with UVES on the Very Large Telescope (VLT), using the iodine cell as a wavelength reference. Again, some time was lost due to the weather (around 25%), including all of night four. The median exposure time was 50 s, with a readout time between exposures of 21 s (Nyquist frequency of about 7000 μ Hz).

To obtain the RV time series, all the individual spectra were reduced following the method described in Butler et al.

Table 1
Atmospheric Parameters Derived from the Spectroscopic Analysis

T_{eff}	4700 ± 65 k
$\log g$	4.50 ± 0.07
[Fe/H]	$-0.17 \pm 0.01 \pm 0.03$
[α /Fe]	$-0.06 \pm 0.03 \pm 0.05$

Note. Note that the quoted uncertainties are internal only (for the abundances; the spread \pm the sensitivity to the other parameters), and g is measured in cm s^{-2} .

(1996, 2004). The RV time series is shown in the bottom panel of Figure 1.

2.3. Spectroscopic Analysis

Some spectra taken as part of the UVES campaign were also used for a spectroscopic analysis. Based on the high S/N iodine-free template spectrum of ϵ Indi A, we were able to derive spectroscopic values of the effective temperature, surface gravity, [Fe/H], and the alpha enhancement using a classical equivalent-width spectral analysis with the line list from Slumstrup et al. (2019). The results are presented in Table 1, with uncertainties internal to the analysis only. The auxiliary program ABUNDANCE within the SPECTRUM software (Gray & Corbally 1994) was used to determine the atmospheric parameters under the assumption of LTE, using ATLAS9 models (Castelli & Kurucz 2003) and solar abundances from Grevesse & Sauval (1998). We used astrophysical oscillator strengths, with the $\log gf$ values for each absorption line adjusted to yield the solar elemental abundances of Grevesse & Sauval (1998). The [α /Fe] in this paper is defined as $\frac{1}{4} \cdot ([\text{Ca}/\text{Fe}] + [\text{Si}/\text{Fe}] + [\text{Mg}/\text{Fe}] + [\text{Ti}/\text{Fe}])$.

ϵ Indi A has been the subject of several previous spectroscopic analyses, dating as far back as 1980 (for an overview, visit, for instance, Simbad).¹⁹ The star is reported to be metal-poor, with a median [Fe/H] = -0.16 dex, which is in excellent agreement with our determination from the UVES spectrum. Median values of the effective temperature ($T_{\text{eff}} = 4649$ K) and surface gravity ($\log g = 4.54$) are also in agreement with our determined values. Based on abundances from the literature (Kollatschny 1980; Adibekyan et al. 2012; Delgado Mena et al. 2017; Luck 2018; Soto & Jenkins 2018; Hojjatpanah et al. 2019), it is possible to compute values of the alpha enhancement that can be compared to our value. The median value computed from the literature is [α /Fe] = 0.12, which, in combination with our value, indicates little to no alpha enhancement.

3. Seismic Data Analysis

3.1. Calculation of the Power Spectrum

We calculated weighted power spectra using a standard sine-wave fitting technique (see, e.g., Kjeldsen 1992; Frandsen et al. 1995; Handberg & Lund 2014). The weights were taken as the inverse of the measurement uncertainties, which we estimated as the smoothed scatter in the time series (orange points in Figure 1). The median scatter was 76 cm s^{-1} for UVES and 78 cm s^{-1} for HARPS. The slightly smoothed weighted power spectra for the HARPS and UVES observing runs are shown in the top two panels of Figure 2 (blue lines).

¹⁹ http://simbad.cds.unistra.fr/simbad/sim-id?Ident=%403387848&Name=%2Beps+Ind&submit=display+all+measurements#lab_meas

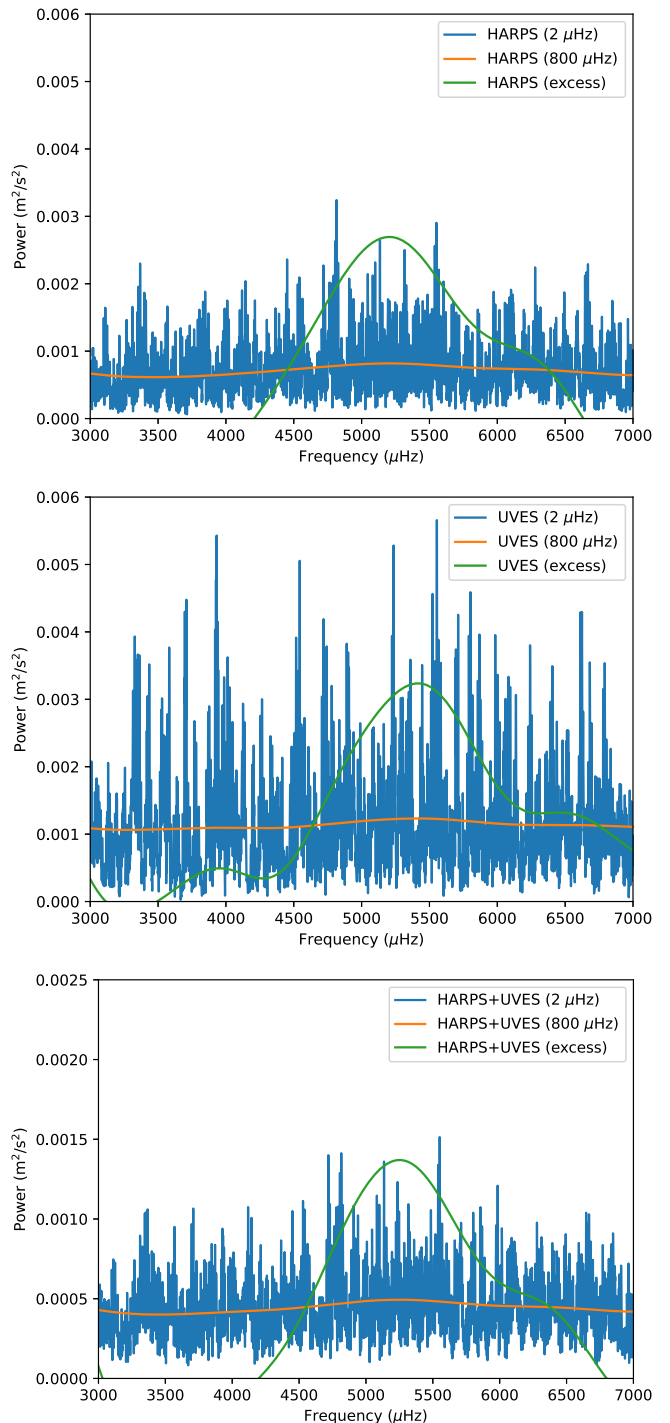


Figure 2. Power spectra of ϵ Indi A from HARPS (top), UVES (middle), and the combined data (bottom; note the different vertical scale). In each panel, the blue curve is the power spectrum smoothed over a width of 2 μHz , the orange curve is smoothed by a width of 800 μHz , and the green curve shows the power excess after subtracting the noise (expanded vertically by a factor of 20 for visibility).

To calculate the power spectrum of the combined HARPS and UVES data we merged them in the time domain, rather than averaging the power spectra, because this allowed us to estimate the spectral window of the combined data (see also Bedding & Kjeldsen 2022). This combined weighted power spectrum, shown in the bottom panel of Figure 2, comprises around 70% power from HARPS and 30% power from UVES.

Table 2

Frequency of Maximum Oscillation Power (ν_{\max}) and Amplitudes of the Central $\ell = 0$ Mode of ϵ Indi A (Corrected for Apodization)

Quantity	Symbol	Data Set	Value
Frequency of maximum power	ν_{\max}	UVES	$5440 \pm 170 \mu\text{Hz}$
		HARPS	$5210 \pm 145 \mu\text{Hz}$
		Combined	$5265 \pm 110 \mu\text{Hz}$
Peak amplitude	$A(\ell = 0 \text{ at peak})$	UVES	$3.1 \pm 0.9 \text{ cm/s}$
		HARPS	$3.6 \pm 0.7 \text{ cm/s}$
		Combined	$3.4 \pm 0.6 \text{ cm/s}$

3.2. Location of the Power Envelope and Mode Amplitude

To determine the frequency of maximum oscillation power, ν_{\max} , and to estimate the amplitude of the oscillations, we followed the method described by Kjeldsen et al. (2005, 2008). This involves the following steps: (i) remove the structure from individual p -modes in the power spectrum by heavily smoothing with a Gaussian with a FWHM of $800 \mu\text{Hz}$ ($\sim 4\Delta\nu$, with $\Delta\nu$ being the expected large frequency separation; orange curves in Figure 2); (ii) convert to power density by multiplying by the effective length of the observing run (calculated as the reciprocal of the area under the spectral window in power); and (iii) fit and subtract the background noise using a linear fit to the area surrounding the power envelope (orange curves in Figure 2). From this, ν_{\max} can be found as the peak position.

A last step is needed to extract the mode amplitude, namely (iv) multiply by 4.09 (the effective number of modes per order) and take the square root, in order to convert to amplitude per oscillation mode.

4. Results

4.1. Measurement of ν_{\max}

The determined center of the power excess (ν_{\max}) as well as the amplitude of the central radial mode (with degree $\ell = 0$) can be found for the HARPS, UVES, and combined power spectra in Table 2. The main source of uncertainty for ν_{\max} and the peak amplitude is the noise background. We estimated the error bars for the three excess power estimates by making simple simulations with a known input, using the same spectral window and S/N as the real data. In the following, we chose to use the ν_{\max} from the combined power spectrum as this is based on the most data, which is a choice in line with our previous multisite campaigns to detect solar-like oscillations (e.g., Kjeldsen et al. 2005; Bedding et al. 2006, 2007; Arentoft et al. 2008).

As an effect of the nonzero exposure time, the mode amplitudes will decrease slightly and the frequency of maximum power will shift to lower frequencies; an effect sometimes referred to as apodization (for the effect on mode amplitudes see, e.g., Chaplin et al. 2011b; Kallinger et al. 2014). To understand this effect, all three data sets (HARPS, UVES, and the combined) were simulated 100 times with the actual exposure times and using the individual statistical weights. The effect for the three data sets—based on simulating a p -mode excess power envelope at $5250 \mu\text{Hz}$ —is that, to account for the nonzero exposure times, the measured peak amplitudes should be increased by 4.2% (HARPS), 12.2%

(UVES), and 6.8% (combined), while the ν_{\max} values should be increased by 0.1% (HARPS), 0.4% (UVES), and 0.2% (combined). While the shift of ν_{\max} is well below the uncertainty, the effect on the amplitude is relatively larger, although still below the uncertainty of the amplitude estimate. These corrections have been applied in Table 2.

4.2. Mass of ϵ Indi A

As mentioned in Section 1, it is common to estimate the mass of a star with solar-like oscillations from ν_{\max} and $\Delta\nu$ using the asteroseismic scaling relations. However, if a reliable luminosity or radius is available, the mass can be estimated from ν_{\max} without requiring $\Delta\nu$, as has been done in studies of red giants (Stello et al. 2008; Hon et al. 2021). Based on the frequency of maximum power (Table 2), the effective temperature (Table 1), as well as the computed radius from combining the distance with the measured angular diameter, we can calculate the mass of ϵ Indi A using the scaling relations (see, e.g., Brown et al. 1991; Kjeldsen & Bedding 1995). Specifically, the mass can be found as (Stello et al. 2008; Kallinger et al. 2010)

$$\frac{M}{M_{\odot}} \approx \left(\frac{\nu_{\max}}{\nu_{\max,\odot}} \right) \left(\frac{R}{R_{\odot}} \right)^2 \left(\frac{T_{\text{eff}}}{T_{\text{eff},\odot}} \right)^{0.5}, \quad (1)$$

with suitable solar reference values. In this work we adopt $\nu_{\max,\odot} = 3090 \pm 30 \mu\text{Hz}$ (Huber et al. 2011) and $T_{\text{eff},\odot} = 5772.0 \pm 0.8 \text{ K}$ (Prša et al. 2016). To obtain the radius of ϵ Indi A we used the distance from the astrophysical parameters table of Gaia DR3 (Creevey et al. 2023): $d = 3.648^{+0.022}_{-0.009} \text{ pc}$ (DISTANCE_GSPPHOT). Combining this with the limb-darkened angular diameter of $\theta_{\text{LD}} = 1.817 \pm 0.013 \text{ mas}$ (Rains et al. 2020) gives a radius of $0.713 \pm 0.006 R_{\odot}$, in excellent agreement with the value found by Rains et al. (2020). Using Equation (1) yields a stellar mass of $0.782 \pm 0.023 M_{\odot}$. This is in agreement with the mass of 0.762 ± 0.038 found by Demory et al. (2009) using the interferometric radius and mass–luminosity relationship from Xia et al. (2008).

4.3. Mode Amplitude Variation with the Activity Cycle

We see indications of a difference between the mode amplitudes observed in the HARPS and UVES time series (see Table 2). This is not surprising as the two time series are separated by a time period of a decade, and the mode amplitudes in the Sun are known to vary over its 11 yr activity cycle (Chaplin et al. 2000; Kjeldsen et al. 2008; Kim & Chang 2022).

In fact, making use of 4293 HARPS archival data obtained for ϵ Indi A between 2003 and 2016, binned to 112 nights, we can place our observations in the context of the activity cycle of ϵ Indi A. From the HARPS archival data, we obtained the $\log R'_{\text{HK}}$ values (following Gomes da Silva et al. 2018, 2021) and used those to model the activity cycle of ϵ Indi A. Figure 3 shows the variation of $\log R'_{\text{HK}}$ phase-folded onto the estimated cycle period of ~ 2600 days. The scatter of the HARPS observations about the sinusoidal model is caused by rotational activity variations.

As can be seen from the figure, we happened to observe ϵ Indi A both near the minimum (HARPS) and near the

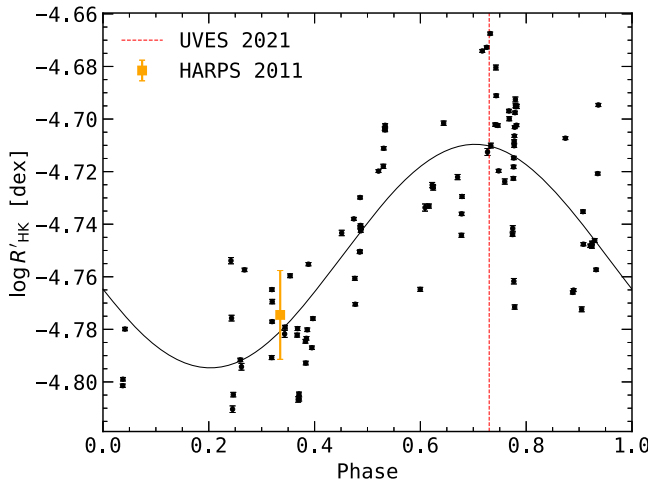


Figure 3. Phase-folded activity cycle of ϵ Indi A from $\log R'_{\text{HK}}$. The black dots show the HARPS observations with our seismic campaign marked in yellow (error bar given by the standard deviation of the observations taken during the campaign). The red dotted line indicates the time of our UVES seismic observations, where the Ca-II H and K lines were not measured, and the solid black line represents a simple sinusoidal variation of $\log R'_{\text{HK}}$ with a period of 2600 days.

maximum (UVES) of activity. The difference between our two measurements of the oscillation amplitude is only marginally significant (Table 2), but it is noteworthy that it is consistent with expectations of an inverse correlation with activity.

5. Conclusions

We have detected solar-like oscillations in the K5 dwarf ϵ Indi A. Our measured value of ν_{max} of $5265 \pm 110 \mu\text{Hz}$ is the highest so far found for solar-like oscillations, surpassing Kepler-444 (K0 V; $4540 \mu\text{Hz}$; Campante et al. 2015), τ Ceti (G8 V; $4490 \mu\text{Hz}$; Teixeira et al. 2009), and α Cen B (K1 V; $4090 \mu\text{Hz}$; Kjeldsen et al. 2005). Combining this detection with a known distance and angular diameter, we estimate the mass of ϵ Indi A to be $0.782 \pm 0.023 M_{\odot}$, in agreement with the literature values. In addition, we see indications of the expected inverse correlation between the activity cycle and the observed mode amplitudes. This result paves the way for detections of solar-like oscillations in more early-to-mid K-dwarfs.

Acknowledgments

Based on observations collected at the European Southern Observatory under ESO programmes 087.D-0511 and 105.20CY. This work was supported by a research grant (42101) from VILLUM FONDEN as well as The Independent Research Fund Denmark’s Inge Lehmann program (grant agreement No. 1131-00014B). Funding for the Stellar Astrophysics Centre was provided by The Danish National Research Foundation (grant agreement No. DNRF106). T.R.B. is supported by an Australian Research Council Laureate Fellowship (FL220100117). T.L.C. is supported by Fundação para a Ciência e a Tecnologia (FCT) in the form of a work contract (CEECIND/00476/2018). J.G.S. acknowledges support from the Fundação para a Ciência e a Tecnologia (FCT) research grants UIDB/04434/2020 and UIDP/04434/2020, and 2022.04416.PTDC. This work was cofunded by the European Union (ERC, FIERCE, 101052347). Views and opinions expressed are, however, those of the author(s) only and do not necessarily reflect those of the European Union or the

European Research Council. Neither the European Union nor the granting authority can be held responsible for them. C.A. received funding from the European Research Council (ERC) under the Horizon Europe program (Synergy grant agreement No. 101071505: 4D-STAR). D.S. is supported by the Australian Research Council Discovery grant (DP190100666). This research has made use of the SIMBAD database, operated at CDS, Strasbourg, France. This work has made use of data from the European Space Agency (ESA) mission Gaia (<https://www.cosmos.esa.int/gaia>), processed by the Gaia Data Processing and Analysis Consortium (DPAC, <https://www.cosmos.esa.int/web/gaia/dpac/consortium>). Funding for the DPAC has been provided by national institutions, in particular, the institutions participating in the Gaia Multilateral Agreement. We thank the referee for helpful comments.

Facilities: ESO:3.6m (HARPS), VLT:Kueyen (UVES).

ORCID iDs

- Mia S. Lundkvist <https://orcid.org/0000-0002-8661-2571>
- Hans Kjeldsen <https://orcid.org/0000-0002-9037-0018>
- Timothy R. Bedding <https://orcid.org/0000-0001-5222-4661>
- Mark J. McCaughrean <https://orcid.org/0000-0002-1452-5268>
- R. Paul Butler <https://orcid.org/0000-0003-1305-3761>
- Ditte Slumstrup <https://orcid.org/0000-0003-4538-9518>
- Tiago L. Campante <https://orcid.org/0000-0002-4588-5389>
- Conny Aerts <https://orcid.org/0000-0003-1822-7126>
- Torben Arentoft <https://orcid.org/0000-0002-4696-6041>
- Fabien Carrier <https://orcid.org/0009-0005-1167-0311>
- Laird M. Close <https://orcid.org/0000-0002-2167-8246>
- João Gomes da Silva <https://orcid.org/0000-0001-8056-9202>
- Thomas Kallinger <https://orcid.org/0000-0003-3627-2561>
- Robert R. King <https://orcid.org/0000-0002-9573-2567>
- Yaguang Li (李亚光) <https://orcid.org/0000-0003-3020-4437>
- Simon J. Murphy <https://orcid.org/0000-0002-5648-3107>
- Jakob L. Rørsted <https://orcid.org/0000-0001-9234-430X>
- Dennis Stello <https://orcid.org/0000-0002-4879-3519>

References

- Adibekyan, V. Z., Sousa, S. G., Santos, N. C., et al. 2012, *A&A*, **545**, A32
- Arentoft, T., Kjeldsen, H., Bedding, T. R., et al. 2008, *ApJ*, **687**, 1180
- Auvergne, M., Bodin, P., Boisnard, L., et al. 2009, *A&A*, **506**, 411
- Baglin, A., Auvergne, M., Boisnard, L., et al. 2006b, in COSPAR Scientific Assembly 36, The CoRoT Mission Pre-Launch Status - Stellar Seismology and Planet Finding, 3749
- Baglin, A., Michel, E., Auvergne, M. & COROT Team 2006a, in Proc. of SOHO 18/GONG 2006/HELAS I 624, Beyond the Spherical Sun, ed. K. Fletcher & M. Thompson (ESA Special Publication), 34
- Barnes, S. A. 2007, *ApJ*, **669**, 1167
- Bedding, T. R., Butler, R. P., Carrier, F., et al. 2006, *ApJ*, **647**, 558
- Bedding, T. R., & Kjeldsen, H. 2022, *RNAAS*, **6**, 202
- Bedding, T. R., Kjeldsen, H., Arentoft, T., et al. 2007, *ApJ*, **663**, 1315
- Borucki, W. J., Koch, D., Basri, G., et al. 2010, *Sci*, **327**, 977
- Brown, T. M., Gilliland, R. L., Noyes, R. W., & Ramsey, L. W. 1991, *ApJ*, **368**, 599
- Butler, R. P., Bedding, T. R., Kjeldsen, H., et al. 2004, *ApJL*, **600**, L75
- Butler, R. P., Marcy, G. W., Williams, E., et al. 1996, *PASP*, **108**, 500
- Campante, T. L., Barclay, T., Swift, J. J., et al. 2015, *ApJ*, **799**, 170
- Cannon, R. D. 1970, *MNRAS*, **150**, 111
- Cardoso, C. V., McCaughrean, M. J., King, R. R., et al. 2010, *HiA*, **15**, 761

- Castelli, F., & Kurucz, R. L. 2003, in Proc. of the Symp. of the IAU 210, Modelling of Stellar Atmospheres, Poster Contributions, ed. N. Piskunov, W. W. Weiss, & D. F. Gray (San Francisco, CA: ASP), A20
- Chaplin, W. J., Elsworth, Y., Isaak, G. R., Miller, B. A., & New, R. 2000, *MNRAS*, **313**, 32
- Chaplin, W. J., Kjeldsen, H., Bedding, T. R., et al. 2011b, *ApJ*, **732**, 54
- Chaplin, W. J., Kjeldsen, H., Christensen-Dalsgaard, J., et al. 2011a, *Sci*, **332**, 213
- Chaplin, W. J., & Miglio, A. 2013, *ARA&A*, **51**, 353
- Chen, M., Li, Y., Brandt, T. D., et al. 2022, *AJ*, **163**, 288
- Creevey, O. L., Sordo, R., Pailler, F., et al. 2023, *A&A*, **674**, A26
- Delgado Mena, E., Tsantaki, M., Adibekyan, V. Z., et al. 2017, *A&A*, **606**, A94
- Demory, B.-O., Ségransan, D., Forveille, T., et al. 2009, *A&A*, **505**, 205
- Dieterich, S. B., Weinberger, A. J., Boss, A. P., et al. 2018, *ApJ*, **865**, 28
- Feng, F., Anglada-Escudé, G., Tuomi, M., et al. 2019, *MNRAS*, **490**, 5002
- Feng, F., Butler, R. P., Vogt, S. S., Holden, B., & Rui, Y. 2023, *MNRAS*, **525**, 607
- Frandsen, S., Jones, A., Kjeldsen, H., et al. 1995, *A&A*, **301**, 123
- García, R. A., & Ballot, J. 2019, *LRSP*, **16**, 4
- Gilliland, R. L., Brown, T. M., Christensen-Dalsgaard, J., et al. 2010, *PASP*, **122**, 131
- Gomes da Silva, J., Figueira, P., Santos, N., & Faria, J. 2018, *JOSS*, **3**, 667
- Gomes da Silva, J., Santos, N. C., Adibekyan, V., et al. 2021, *A&A*, **646**, A77
- Gray, R. O., & Corbally, C. J. 1994, *AJ*, **107**, 742
- Grevesse, N., & Sauval, A. J. 1998, *SSRv*, **85**, 161
- Handberg, R., & Lund, M. N. 2014, *MNRAS*, **445**, 2698
- Hekker, S., & Christensen-Dalsgaard, J. 2017, *A&ARv*, **25**, 1
- Hojjatpanah, S., Figueira, P., Santos, N. C., et al. 2019, *A&A*, **629**, A80
- Hon, M., Huber, D., Kuszlewicz, J. S., et al. 2021, *ApJ*, **919**, 131
- Huber, D., Bedding, T. R., Stello, D., et al. 2011, *ApJ*, **743**, 143
- Jackiewicz, J. 2021, *FrASS*, **7**, 102
- Joergens, V., & Reffert, S. 2014, *MmSAI*, **85**, 678
- Kallinger, T., De Ridder, J., Hekker, S., et al. 2014, *A&A*, **570**, A41
- Kallinger, T., Weiss, W. W., Barban, C., et al. 2010, *A&A*, **509**, A77
- Kasper, M., Burrows, A., & Brandner, W. 2009, *ApJ*, **695**, 788
- Kim, K.-B., & Chang, H.-Y. 2022, *NewA*, **92**, 101720
- King, R. R., McCaughrean, M. J., Homeier, D., et al. 2010, *A&A*, **510**, A99
- Kjeldsen, H. 1992, PhD thesis, Aarhus Univ.
- Kjeldsen, H., & Bedding, T. R. 1995, *A&A*, **293**, 87
- Kjeldsen, H., Bedding, T. R., Arentoft, T., et al. 2008, *ApJ*, **682**, 1370
- Kjeldsen, H., Bedding, T. R., Butler, R. P., et al. 2005, *ApJ*, **635**, 1281
- Koch, D. G., Borucki, W. J., Basri, G., et al. 2010, *ApJL*, **713**, L79
- Kollatschny, W. 1980, *A&A*, **86**, 308
- Lachaume, R., Dominik, C., Lanz, T., & Habing, H. J. 1999, *A&A*, **348**, 897
- Luck, R. E. 2018, *AJ*, **155**, 111
- Mainzer, A. K., Roellig, T. L., Saumon, D., et al. 2007, *ApJ*, **662**, 1245
- McCaughrean, M. J., Close, L. M., Scholz, R.-D., et al. 2004, *A&A*, **413**, 1029
- Pathak, P. 2021, *A&A*, **652**, A121
- Prša, A., Harmanec, P., Torres, G., et al. 2016, *AJ*, **152**, 41
- Rains, A. D., Ireland, M. J., White, T. R., Casagrande, L., & Karovicova, I. 2020, *MNRAS*, **493**, 2377
- Reiners, A., Homeier, D., Hauschildt, P. H., & Allard, F. 2007, *A&A*, **473**, 245
- Ricker, G. R., Winn, J. N., Vanderspek, R., et al. 2015, *JATIS*, **1**, 014003
- Rocha-Pinto, H. J., Castilho, B. V., & Maciel, W. J. 2002, *A&A*, **384**, 912
- Roellig, T. L., Van Cleve, J. E., Sloan, G. C., et al. 2004, *ApJS*, **154**, 418
- Scholz, R.-D., McCaughrean, M. J., Lodieu, N., & Kuhlbrodt, B. 2003, *A&A*, **398**, L29
- Slumstrup, D., Grundahl, F., Silva Aguirre, V., & Brogaard, K. 2019, *A&A*, **622**, A111
- Smith, V. V., Tsuji, T., Hinkle, K. H., et al. 2003, *ApJL*, **599**, L107
- Soto, M. G., & Jenkins, J. S. 2018, *A&A*, **615**, A76
- Stello, D., Bruntt, H., Preston, H., & Buzasi, D. 2008, *ApJL*, **674**, L53
- Teixeira, T. C., Kjeldsen, H., Bedding, T. R., et al. 2009, *A&A*, **494**, 237
- Trifonov, T., Tal-Or, L., Zechmeister, M., et al. 2020, *A&A*, **636**, A74
- Viswanath, G., Janson, M., Dahlqvist, C.-H., et al. 2021, *A&A*, **651**, A89
- Xia, F., Ren, S., & Fu, Y. 2008, *Ap&SS*, **314**, 51